

# Enhancement of polarization and magnetization in polycrystalline magnetoelectric composite

K.P. Jayachandran,<sup>a)</sup> J.M. Guedes, and H.C. Rodrigues

IDMEC, Instituto Superior Técnico, University of Lisbon, Av. Rovisco Pais, 1049-001 Lisbon, Portugal

(Dated: 26 March 2021)

Electrical control of magnetization or magnetic control of polarization offers an extra degree of freedom in materials possessing both electric and magnetic dipole moments *viz.*, magnetoelectric multiferroics. Microstructure with polycrystalline configurations that enhances the overall polarization/magnetization and that outperform single crystalline configurations are identified. The characterization of local fields corresponding to the polycrystal configuration underlines nontrivial role played by randomness in better cross-coupling mediated by anisotropic and asymmetric strains.

The magnetoelectric (ME) effect manifests in the linear relation between the magnetic and electric fields in matter and it causes, for instance, either a magnetization or electrical polarization proportional to applied electric/magnetic fields<sup>1</sup>. Yet, the ME effect is possible only for certain magnetic symmetry classes, akin to piezomagnetism. Set of materials classified as magnetoelectric multiferroics possess both the magnetic and ferroelectric orders in the same phase<sup>2</sup>. Apart from exhibiting functionalities of both the orders, a coupling between the ferri-/ferro-magnetic (FM) and ferroelectric (FE) states enable appearance of novel characteristics not present in either of the states<sup>3</sup>. Nonetheless, simultaneous occurrence of magnetism and ferroelectricity in materials is constrained by the conflicting classic chemical requirements regarding electronic orbital occupancy<sup>4,5</sup>. In such a situation, one should envisage only a moderate ME coupling though<sup>6</sup>. For instance, only few examples exist of materials possessing intrinsic ME coupling at room temperature<sup>7,8</sup>. An unambiguous resolution to circumvent this chemical 'contraindication' is by juxtaposing an FE and FM material artificially into strain-mediated multiphase materials such as composites combining the two phases, that thereby yields substantial ME effect<sup>5,6,9</sup>. Moreover, the composites do not need to adhere to the symmetry restrictions of single phase materials and consequently do possess the freedom of choice from a wide variety of ferroics existing above room temperature. Crystallites of the two phases in an ME composite are assumed to be in good mechanical contact if the two phases are polycrystalline. The change in shape of the FE grains in response to an applied electric field causes the ferro-

magnetic grains to deform, resulting in a change in magnetization<sup>10</sup>.

Magneto-elastic effect by means of strain transfer across the interface of an FM/nonmagnetic bilayer could unleash significant changes in the magnetic properties of the ferromagnet. When an FE material is used as the nonmagnetic layer, strain transfer can be reinforced through the induction by an electric field thanks to the inverse piezoelectric effect prevails in the FE material. This additional strain transfer allows one to manipulate the magnetisation by an electric field<sup>11</sup>. The concept of magnetic information recording and memory device technologies as well as electric-field driven magnetoelastic effects on magnetic anisotropy have attracted much interest recently from both fundamental and technological aspects owing to the said modification accomplished on magnetisation orientation<sup>5,11,12</sup>. Among many FM/FE hybrid structures, perovskite manganites/BTO are the well-suited magnetoelastic heterostructures since transport, magnetic, and electronic properties of perovskite manganites are very sensitive to lattice strain and can be easily integrated with BaTiO<sub>3</sub> (BTO) due to the similar crystal structure<sup>13</sup>. For instance when an electric field is applied to the nanostructured BTO/CFO 1-3 composite, the strain created by the piezoelectric (BTO) matrix couples to the magnetostrictive CFO(CoFe<sub>2</sub>O<sub>4</sub>) pillars and hence the strength of the coupling between the ferroelectricity and magnetism are critically dependent on the anisotropy and crystalline structure of the constituents<sup>14,15</sup>.

In this letter, we would be studying the impact of an applied electrical/magnetic fields on a motley ME composite composed of disparate FE and FM materials. We underscore the significance of heterogeneity of one of the constituent phases, *viz.*, the FE phase by introducing randomness in the mi-

---

<sup>a)</sup>Electronic mail: kpjayachandran@gmail.com

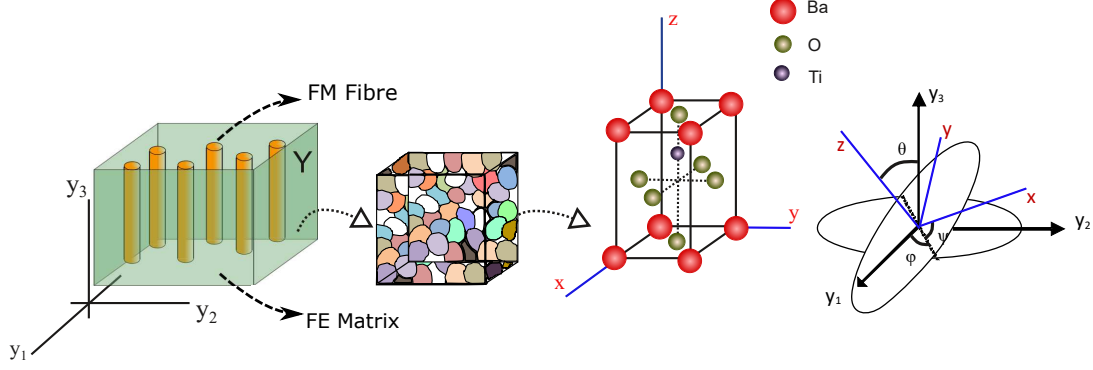


FIG. 1. Schematic hierarchical diagram of the ME multiferroic microstructure browsing through the succession of modeling tasks in the study. The microstructure  $Y$  is a fibre-reinforced ME composite where an FM fibre made of  $\text{CoFe}_2\text{O}_4$  is embedded in a perovskite FE matrix of  $\text{BaTiO}_3$ .  $\text{BaTiO}_3$  is a polycrystal – an aggregate of grains of various orientations (depicted in different colours). The orientation of the grains quantified by the Euler angles  $(\phi, \theta, \psi)$  is in fact that of the underlying crystallographic unit cell and is measured against the microscopic  $(y_1, y_2, y_3)$  coordinate system.

crostructure. Prior research have shown that introducing heterogeneity locally can improve the piezoelectric properties of FE materials and the ensuing coupling effect of the ME composite of which the former is a component<sup>16,17</sup>. Apart from the effect of applied fields, the sway of crystal anisotropy on the polarization/magnetization as demonstrated in various studies<sup>18–21</sup> on magnetoelectric heterostructures is also shown. Another important challenge is to identify the optimum texture and stress level and efficient control of the same to achieve targeted magnetoelectric properties<sup>22</sup>. We demonstrate the effect of local texture in a 1–3 composite, tantamount to the architecture used in Zheng et al.,<sup>14</sup> to map its local field distributions upon applying an external bias field. Moreover, the average polarization and magnetization post application of ample bias fields sufficient to saturate the composite would be computed.

Estimation of the equilibrium macroscopic magneto-electro-electric properties of the ME composite, have been done using the mathematical homogenization method<sup>23,24</sup>. A ME multiferroic composite occupying a volume  $\Omega$  of coordinates  $\mathbf{x}$  (or  $x_i$ ) is considered and the material properties are assumed to change periodically and that period  $\epsilon$  is characterized by the dimension of an elementary cell  $Y$  of coordinates  $\mathbf{y}$  (or  $y_i$ ) of the body (Fig. 1). This lead us to examine fields for unknown physical quantities in the form of two-scale asymptotic expansion in powers of  $\epsilon$  as

$$\zeta^\epsilon(\mathbf{x}) = \zeta^0(\mathbf{x}, \mathbf{y}) + \epsilon \zeta^1(\mathbf{x}, \mathbf{y}), \text{ with } \mathbf{y} = \mathbf{x}/\epsilon \quad (1)$$

and the equivalent macroscopic behaviour is estimated to be first order by the behaviour of  $\zeta^0$ . Here  $\zeta$  stands in lieu of the fields *viz.*,  $\mathbf{u}$ , the displacement,  $\varphi$  and  $\psi$ , the scalar electrical/magnetic potentials respectively of a multiferroic composite<sup>25</sup>. Here the functions  $\zeta^1(\equiv \mathbf{u}^1, \varphi^1 \text{ or } \psi^1)$  are the local variations (or *field perturbations*) describing the heterogeneous part of the solutions and are associated with  $\mathbf{y} = \mathbf{x}/\epsilon$ . Applying calculus of variations, utilising the asymptotic Eq. (1) and its derivatives, the homogenization method essentially culminates in the characterization of effective magneto-electro-elastic moduli when the characteristic length  $\epsilon$  of the period tends to zero. The electrical, magnetic and mechanical fields (*degrees of freedom*) govern the constitutive equations of the linear ME multiferroic solid (see Supplementary material). The model quantifies all the local fields and potentials besides stress ( $\sigma$ ) and strain ( $\epsilon$ ) fields, magnetization (via magnetic flux density,  $\mathbf{B}$ ), polarization (via electric displacement,  $\mathbf{D}$ ) as well as von-Mises stress upon the application of an external field (either electric/magnetic or mechanical). The *macroscopic averages*  $\langle \sigma_{ij} \rangle$ ,  $\langle D_i \rangle$ , and  $\langle B_i \rangle$  can be computed once the homogenized solution for  $\mathbf{u}^0$ ,  $\varphi^0$  and  $\psi^0$  and that of the corresponding fields *viz.*,  $\frac{\partial u_i^0(\mathbf{x})}{\partial x_k}$ ,  $\frac{\partial \varphi^0(\mathbf{x})}{\partial x_j}$  and  $\frac{\partial \psi^0(\mathbf{x})}{\partial x_j}$  are prescribed (see Supplementary material). This *postulate* is equally applicable for the cases when magnetic field  $\mathbf{H} = 0$ , the applied macroscopic electric field  $\langle E_i \rangle$  generates average magnetization<sup>1</sup>

$$\langle M_k \rangle = \tilde{\alpha}_{ik} \langle E_i \rangle \quad (2)$$

and when electric field  $\mathbf{E} = 0$ , the applied macro-

scopic magnetic field  $\langle H_i \rangle$  generates average electrical polarization<sup>1</sup>

$$\langle P_i \rangle = \tilde{\alpha}_{ik} \langle H_k \rangle \quad (3)$$

The FE matrix of the ME composite is composed of polycrystalline BaTiO<sub>3</sub>. The orientation of the BaTiO<sub>3</sub> crystallographic grains in the composite is characterized using Euler angles. It is seen from the Euler angles  $(\phi, \theta, \psi)$  (Fig. 1) that it measure the rotation of the crystallographic coordinates (x, y, z) with reference to the microstructure coordinates  $(y_1, y_2, y_3)$ . The three Euler angles are modelled as statistically distributed in a normal distribution after poling obeying the probability distribution function  $f(\alpha | \mu, \sigma) = 1/(\sigma\sqrt{2\pi})\exp - [(\alpha - \mu)^2/2\sigma^2]$ . Here  $\alpha$  is the random variable representing the orientations (i.e., the Euler angles)  $(\phi, \theta, \psi)$  and  $\mu$  and  $\sigma$  are the mean and the standard deviation, respectively. The fibres embedded in the matrix is composed of the FM material CoFe<sub>2</sub>O<sub>4</sub> which is treated as bulk material without assigning any orientation whatsoever. The numerical model developed is implemented in finite element method. The convergence of piezoelectric properties with unit cell size allows us to determine the simulation-space independent, macroscopic magnetoelectric properties at various distribution of grains (See Supplementary material).

The average magnetic property response along the  $y_3$ -axis of the local coordinates (which was set to align along the normal to the composite plane) consequent to an external biasing electrical field is studied first. Here we apply an electric field ( $E_3$ ) which suffices to saturate the polycrystalline BTO-CFO composite. The results are summarised in Fig. 2. In general, the average fields acting through out-of-plane (the components along  $y_3$ -axis) to the composite plane are greater in magnitude than the other components. Unlike the common perception of great performance of single crystal piezoelectrics, we see much better magnetization  $\langle M_3 \rangle$  while the BTO is still polycrystalline (Fig. 2 and Table I). In Fig. 2 the polycrystalline data of the averages are differentiated from single crystal by painting the single crystal region by a shade. Randomness, introduced by local microstructural heterogeneity could potentially enhance piezoelectricity in relaxor ferroelectric ceramics<sup>16</sup>. Here, we have incorporated randomness in the ferroelectric BTO phase through Euler orientations of the constituent grains kept at a normal distribution but with a standard deviation of  $\mu$  rad. The maximum magnetization  $\langle M_3 \rangle$

TABLE I. Average values of magnetization  $\langle M_3 \rangle$  (in A/m) at constant external electric field, and electric polarization  $\langle P_3 \rangle$  (C/m<sup>2</sup>) at external magnetic field of 1–3 magnetoelectric composite BaTiO<sub>3</sub> (single and polycrystalline)–ceramic CoFe<sub>2</sub>O<sub>4</sub>.

BTO phase	Orientation <sup>a</sup> or ODP <sup>b</sup>	Averages	
		$\langle M_3 \rangle$	$\langle P_3 \rangle$
Single crystalline	(0,0,0)	$2.63 \times 10^4$	0.03
	(0, $\pi/4$ ,0)	$-5.48 \times 10^4$	-0.07
	(0, $\pi/2$ ,0)	-1.39	$-2 \times 10^{-6}$
Polycrystalline	(0, $\frac{1}{2}$ )    (0, $\frac{1}{2}$ )    (0, $\frac{1}{2}$ )	$1.38 \times 10^5$	0.17
	(0,1)    (0,0)    (0,0)	$2.47 \times 10^4$	0.03
	(0,0)    (0,1)    (0,0)	$1.3 \times 10^5$	0.16
	(0,0)    (0,0)    (0,1)	$2.47 \times 10^4$	0.03
	(0,1)    (0,1)    (0,1)	$1.49 \times 10^5$	0.19
	(0, $\pi$ )    (0, $\pi$ )    (0, $\pi$ )	$1.46 \times 10^4$	0.02
Experiment <sup>c</sup>	–	$\approx 3.5 \times 10^5$	$\approx 0.23$
Experiment <sup>d</sup>	–	$\approx 3.15 \times 10^5$	$\approx 0.1$

<sup>a</sup> Euler angles  $(\phi, \theta, \psi)$  (rad) of rotation in single crystal BTO phase

<sup>b</sup> Orientation Distribution Parameters

$(\mu_\phi, \sigma_\phi) || (\mu_\theta, \sigma_\theta) || (\mu_\psi, \sigma_\psi)$  (rad) of polycrystal BTO phase

<sup>c</sup> CoFe<sub>2</sub>O<sub>4</sub> nanopillars embedded BaTiO<sub>3</sub> matrix in a 1–3 composite from Ref. [14].

<sup>d</sup> CoFe<sub>2</sub>O<sub>4</sub>–BaTiO<sub>3</sub> 1–3 nanocomposite from Ref. [26].

is seen for BTO polycrystal phase with orientation distribution parameters  $(\mu_\phi = 0, \sigma_\phi = 1, \mu_\theta = 0, \sigma_\theta = 1, \mu_\psi = 0, \sigma_\psi = 1)$ . Each grain orientation would be dissected and kept separately and the grains are allowed to chose the combination of three  $(\phi, \theta, \psi)$  but dictated by the corresponding mean ( $\mu$ ) and standard deviation ( $\mu$ ). The value of  $\langle M_3 \rangle = 1.49 \times 10^5$  (A/m) obtained here compares with the order of  $\langle M_3 \rangle$  measured by Zheng et al.,<sup>14</sup> on nanostructures with vertically aligned CoFe<sub>2</sub>O<sub>4</sub> nanopillars embedded in BaTiO<sub>3</sub> matrix. Zheng et al. value is the saturation magnetization ( $M_s$ ) response against an applied magnetic field (hysteresis) of the composite rather than the cross coupling magnetization value as is obtained in the present work (Table I) and hence the deviation is obvious. Epitaxial CFO films on BaTiO<sub>3</sub> single crystal substrate shows  $\langle M_3 \rangle \approx 2.5 \times 10^5$  (A/m)<sup>27</sup> under a magnetic field.

The property variation at various configurations (single crystalline data in shaded area) consequent to the application of external magnetic field  $H_3$  are given in Fig. 3. Here the electric field is off and hence the electrical responses are dictated solely by the piezomagnetic effect of the CFO component of

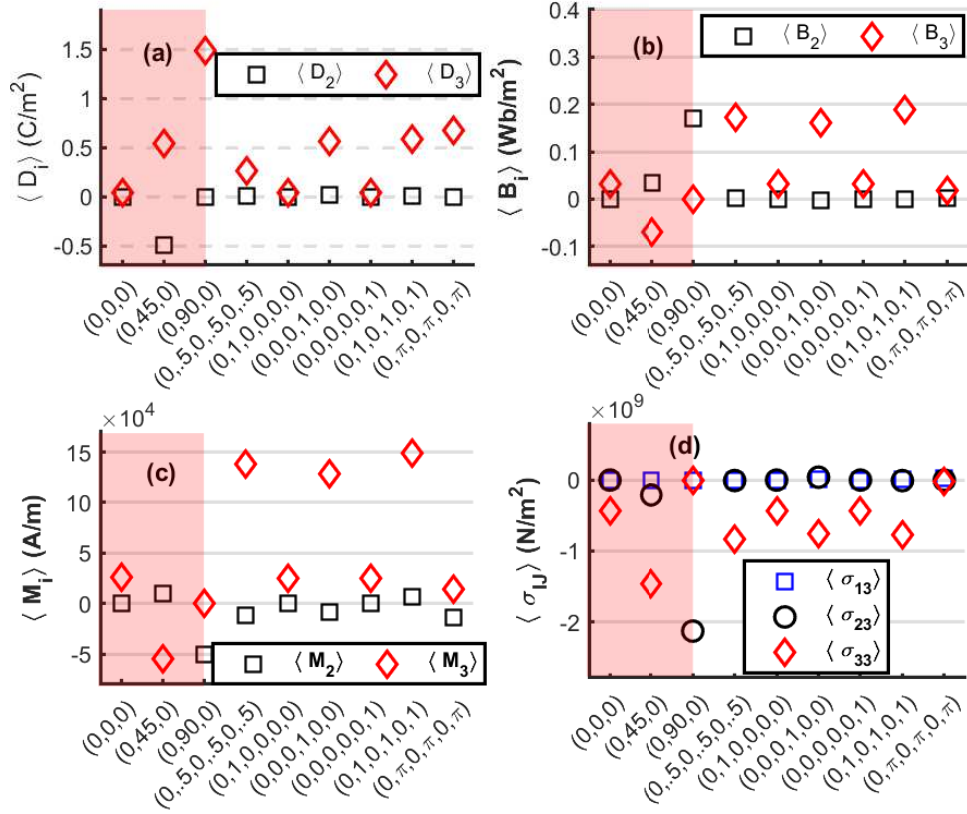


FIG. 2. Average fields for the multiferroic ME 1–3 composite BTO–CFO. (a) shows the average dielectric displacement  $\langle D_i \rangle$ . (b) is the average magnetic flux density,  $\langle B_i \rangle$  (c) shows the average magnetization  $\langle M_i \rangle$  and (d) show the relevant tensor components of the average stress  $\langle \sigma_{IJ} \rangle$  upon applying an external electric field  $\langle E_3 \rangle$  along the  $y_3$ -axis of the composite (i.e., along the normal to the composite plane). The data fall in the shaded area corresponds to single crystal BTO matrix–polycrystalline CFO fibre constituting the ME composite. The BTO orientations in Euler angles  $(\phi^\circ, \theta^\circ, \psi^\circ)$  are marked along the horizontal axis in the shaded area. Rest of the data correspond to polycrystalline ME composite with BTO orientation distribution  $(\mu_\phi, \sigma_\phi, \mu_\theta, \sigma_\theta, \mu_\psi, \sigma_\psi)$  (along the horizontal axis). Here the x-axis is representative line separating the quantities plotted on the y-axis. i.e., the data points in the plot have no abscissae.

the ME composite. More precisely, the emergence of electrical displacement  $\langle D_j \rangle$  (Fig. 3) which bears the signature of polarization and the electrical polarization  $\langle P_j \rangle$  (Fig. 3 and Table I) itself. The average polarization out-of-plane of the composite layer  $\langle P_3 \rangle$  peaks at the polycrystal phase of BTO as seen in magnetization  $\langle M_3 \rangle$  in the previous simulation experiment with applied electric field (Fig. 2). The polarization  $\langle P_3 \rangle$  compares well with the experiments (Table I)

The causal relationship between local microstructure and better magnetic response of polycrystalline BTO–CFO composite can be explored from mapping the local field distribution in response to the external field. The average or macroscopic field applied

to a magnetoelectric composite would permeate the material microstructure and would spread unequally into different points owing to the heterogeneity of the material. The anisotropy due to the underlying crystalline structure of the constituent phases contribute to this phenomenon. The associated local field distribution exhibit spacial fluctuations critical to coupling phenomena. The stress/strain mediating the coupling phenomenon is spread non-uniformly across the microstructure as is seen (in Fig. S??) in Supplementary material. The equivalent von Mises stress indicates a stress concentration across BTO matrix compared to the CFO fibre. This is reflected and underlined in the variation of microscopic displacement  $\mathbf{u}^\epsilon$  (see Fig. S??). The

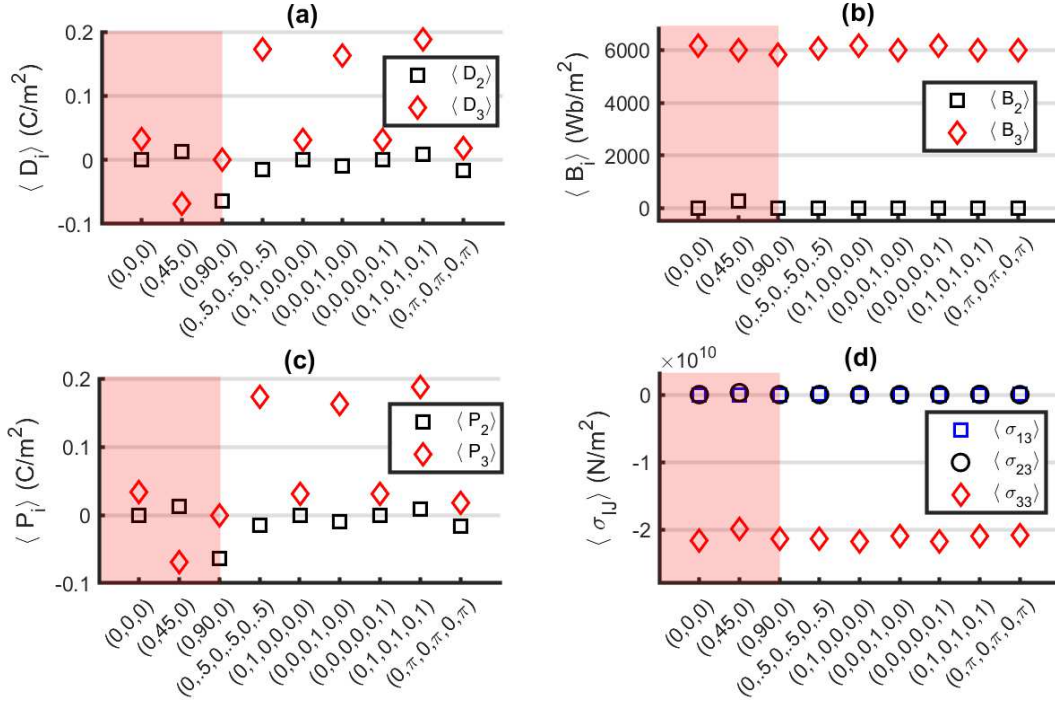


FIG. 3. Average fields for the multiferroic ME 1–3 composite BTO–CFO. (a) shows the average dielectric displacement  $\langle D_i \rangle$ . (b) is the average magnetic flux density,  $\langle B_i \rangle$  (c) shows the average magnetization  $\langle M_i \rangle$  and (d) show the relevant tensor components of the average stress  $\langle \sigma_{IJ} \rangle$  upon applying an external magnetic field  $\langle H_3 \rangle$  along the  $y_3$ -axis of the composite (i.e., along the normal to the composite plane). Here the x-axis is representative line separating the quantities plotted on the y-axis. i.e., the data points in the plot have no abscissae.

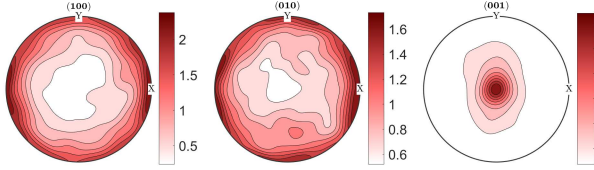


FIG. 4. Pole figures (contour plots) of the polycrystalline BTO matrix while the ODPs are  $(\mu_\phi = 0, \sigma_\phi = 1, \mu_\theta = 0, \sigma_\theta = 1, \mu_\psi = 0, \sigma_\psi = 1)$ . At this configuration, the ME composite deliver maximum  $\langle M_3 \rangle$  and  $\langle P_3 \rangle$ .

asymmetry and anisotropy of the local stress/strain distributed across the microstructure could be seen in histograms (Fig. S??). The in-plane strain  $\epsilon_{12}^\epsilon$  records values orders of magnitude greater than other components (Fig. S??) conforming the compression of the composite in  $x$  and  $y$  directions<sup>26</sup>. The cross-coupling effect of the applied electric field

results in appreciable local magnetic potential  $\psi^\epsilon$  and associated magnetism (Fig. S??). The magnetic field induced local profile of fields are shown in the Supplementary materials. It reinforces the cross-coupling between the magnetic and electric degrees of freedom through mechanical stress. The pole figure in Fig. 4 shows the distribution of grain orientation about the  $y_3$ -axis (or  $z$ -axis) of the composite structure. The  $\langle 001 \rangle$  axes of the ferroelectric BTO (where the spontaneous polarization is oriented) is aligned mostly along the  $y_3$ -axis (here the  $[001]$  pseudo cubic axes of BTO is directed out-of-plane).

In summary, strong magnetoelectric coupling is resulted while a polycrystalline ME composite of 1–3 BaTiO<sub>3</sub>–CoFe<sub>2</sub>O<sub>4</sub> is subjected external electric/magnetic fields. In contrast to single crystal BaTiO<sub>3</sub>–polycrystal CoFe<sub>2</sub>O<sub>4</sub> composite, the averages of polarization and magnetization of the polycrystalline BaTiO<sub>3</sub>–CoFe<sub>2</sub>O<sub>4</sub> exceeds that of the single crystal version. The depiction of local fields corresponding to the polycrystal configuration suggests

nontrivial role played by randomness in better cross-coupling mediated by anisotropic and asymmetric strains.

## I. ACKNOWLEDGMENTS

This work was supported by FCT-Fundação para a Ciência e a Tecnologia, through IDMEC, under LAETA, project UIDB/50022/2020.

- <sup>1</sup>L. D. Landau and E. M. Lifshitz, *Electrodynamics of Continuous Media* (Pergamon, Oxford, 1960).
- <sup>2</sup>H. Schmid, “Multiferroic magnetoelectrics,” *Ferroelectrics* **162**, 317–338 (1994).
- <sup>3</sup>M. Fiebig, T. Lottermoser, D. Meier, and M. Trassin, “The evolution of multiferroics,” *Nat. Rev. Mater.* **1**, 16046 (2016).
- <sup>4</sup>N. A. Hill, “Why are there so few magnetic ferroelectrics?” *J. Phys. Chem. B* **104**, 6694–6709 (2000).
- <sup>5</sup>N. A. Spaldin and R. Ramesh, “Advances in magnetoelectric multiferroics,” *Nat Mater* **18**, 203–212 (2019).
- <sup>6</sup>S.-W. Cheong and M. Mostovoy, “Multiferroics: a magnetic twist for ferroelectricity,” *Nat Mater* **6**, 13–20 (2007).
- <sup>7</sup>P. Mandal, M. J. Pitcher, J. Alaria, H. Niu, P. Borisov, P. Stamenov, J. B. Claridge, and M. J. Rosseinsky, “Designing switchable polarization and magnetization at room temperature in an oxide,” *Nature* **525**, 363–366 (2015).
- <sup>8</sup>J. Long, M. S. Ivanov, V. A. Khomchenko, E. Mamtova, J.-M. Thibaud, J. Rouquette, M. Beauduin, D. Granier, R. A. S. Ferreira, L. D. Carlos, B. Donnadieu, M. S. C. Henriques, J. A. Paixão, Y. Guari, and J. Larionova, “Room temperature magnetoelectric coupling in a molecular ferroelectric ytterbium(iii) complex,” *Science* **367**, 671–676 (2020).
- <sup>9</sup>M. Avellaneda and G. Harsh, “Magnetoelectric effect in piezoelectric magnetostrictive multilayer (2–2) composites,” *J. Intell. Mater. Syst. Struct.* **5**, 501–513 (1994).
- <sup>10</sup>J. van den Boomgaard and R. A. J. Born, “A sintered magnetoelectric composite material BaTiO<sub>3</sub>-Ni(Co, Mn)Fe<sub>2</sub>O<sub>4</sub>,” *J. Mater. Sci.* **13**, 1538–1548 (1978).
- <sup>11</sup>T. Taniyama, “Electric-field control of magnetism via strain transfer across ferromagnetic/ferroelectric interfaces,” *J Phys-Condens Mat* **27**, 504001 (2015).
- <sup>12</sup>C. W. Nan, M. I. Bichurin, S. Dong, D. Viehland, and G. Srinivasan, “Multiferroic magnetoelectric composites: Historical perspective, status, and future directions,” *J. Appl. Phys* **103**, 031101 (2008).
- <sup>13</sup>G. Panchal, D. M. Phase, V. R. Reddy, and R. J. Choudhary, “Strain-induced elastically controlled magnetic anisotropy switching in epitaxial La<sub>0.7</sub>Sr<sub>0.3</sub>MnO<sub>3</sub> thin films on BaTiO<sub>3</sub>(001),” *Phys. Rev. B* **98**, 045417 (2018).
- <sup>14</sup>H. Zheng, J. Wang, S. E. Lofland, Z. Ma, L. Mohaddes-Ardabili, T. Zhao, L. Salamanca-Riba, S. R. Shinde, S. B. Ogale, F. Bai, D. Viehland, Y. Jia, D. G. Schlom, M. Wuttig, A. Roytburd, and R. Ramesh, “Multiferroic BaTiO<sub>3</sub>-CoFe<sub>2</sub>O<sub>4</sub> nanostructures,” *Science* **303**, 661–663 (2004).
- <sup>15</sup>H. Zheng, J. Kreisel, Y.-H. Chu, R. Ramesh, and L. Salamanca-Riba, “Heteroepitaxially enhanced magnetic anisotropy in batio<sub>3</sub>-cofe<sub>2</sub>o<sub>4</sub> nanostructures,” *Appl Phys Lett* **90**, 113113 (2007).
- <sup>16</sup>F. Li, D. Lin, Z. Chen, Z. Cheng, J. Wang, C. Li, Z. Xu, Q. Huang, X. Liao, L.-Q. Chen, T. R. Shrout, and S. Zhang, “Ultrahigh piezoelectricity in ferroelectric ceramics by design,” *Nat Mater* **17**, 349–354 (2018).
- <sup>17</sup>K. P. Jayachandran, J. M. Guedes, and H. C. Rodrigues, “Piezoelectricity enhancement in ferroelectric ceramics due to orientation,” *Appl. Phys. Lett.* **92**, 232901 (2008).
- <sup>18</sup>S. Sahoo, S. Polisetty, C.-G. Duan, S. S. Jaswal, E. Y. Tsymbal, and C. Binck, “Ferroelectric control of magnetism in BaTiO<sub>3</sub>-Fe heterostructures via interface strain coupling,” *Phys. Rev. B* **76**, 092108 (2007).
- <sup>19</sup>X. Han, L. Xi, Y. Li, X. Guo, D. Li, Z. Wang, Y. Zuo, and D. Xue, “Demonstration of magnetoelectric memory cell in (110) [pb(mg<sub>1</sub>/2nb<sub>2</sub>/3)o<sub>3</sub>]0.68-[pbtio<sub>3</sub>]0.32/ru/feco heterostructures,” *Appl Phys Lett* **105**, 122402 (2014).
- <sup>20</sup>S. Zhang, Y. Zhao, X. Xiao, Y. Wu, S. Rizwan, L. Yang, P. Li, J. Wang, M. Zhu, H. Zhang, X. Jin, and X. Han, “Giant electrical modulation of magnetization in Co<sub>4</sub>Fe<sub>40</sub>B<sub>20</sub>/Pb(Mg<sub>1</sub>/3Nb<sub>2</sub>/3)0.7Ti<sub>0.3</sub>O<sub>3</sub>(011) heterostructure,” *Sci Rep* **4**, 3727 (2014).
- <sup>21</sup>W. P. Zhou, Q. Li, Y. Q. Xiong, Q. M. Zhang, D. H. Wang, Q. Q. Cao, L. Y. Lv, and Y. W. Du, “Electric field manipulation of magnetic and transport properties in SrRuO<sub>3</sub>/Pb(Mg<sub>1</sub>/3Nb<sub>2</sub>/3)O<sub>3</sub>-PbTiO<sub>3</sub> heterostructure,” *Sci Rep* **4**, 6991 (2014).
- <sup>22</sup>S. Stephen, “Multiferroics and the path to the market,” (2019), Nian Sun, professor at Northeastern University, talks to Nature Materials about the potential applications of multiferroic materials.(<https://doi.org/10.1038/s41563-019-0295-6>).
- <sup>23</sup>E. Sanchez-Palencia, *Non-homogeneous media and vibration theory, Lecture notes in physics 127* (Springer-Verlag, Berlin, 1980).
- <sup>24</sup>K. P. Jayachandran, J. M. Guedes, and H. C. Rodrigues, “Homogenization method for microscopic characterization of the composite magnetoelectric multiferroics,” *Sci Rep* **10**, 1276 (2020).
- <sup>25</sup>K. P. Jayachandran, J. M. Guedes, and H. C. Rodrigues, “A generic homogenization model for magnetoelectric multiferroics,” *J Intel Mat Syst Str* **25**, 1243–1255 (2014).
- <sup>26</sup>C. Schmitz-Antoniak, D. Schmitz, P. Borisov, F. M. F. de Groot, S. Stienen, A. Warland, B. Krumme, R. Feyerherm, E. Dudzik, W. Kleemann, and H. Wende, “Electric in-plane polarization in multiferroic cofe<sub>2</sub>o<sub>4</sub>/batio<sub>3</sub> nanocomposite tuned by magnetic fields,” *Nat Commun* **4**, 2051 (2013).
- <sup>27</sup>R. V. Chopdekar and Y. Suzuki, “Magnetoelectric coupling in epitaxial cofe<sub>2</sub>o<sub>4</sub> on batio<sub>3</sub>,” *Appl Phys Lett* **89**, 182506 (2006), <https://doi.org/10.1063/1.2370881>.

# Supplementary material to 'Enhancement of polarization and magnetization in polycrystalline magnetoelectric composite'

K.P. Jayachandran,\* J.M. Guedes, and H.C. Rodrigues  
 IDMEC, Instituto Superior Técnico, Universidade de Lisboa,  
 Lisboa, Av. Rovisco Pais, 1049-001 Lisbon, Portugal

This supporting material for the work on microscopic characterization of the composite polycrystalline magnetoelectric multiferroics include Literature review, theory of homogenization, its numerical implementation and few key results.

## I. INTRODUCTION

The materials classified as magnetoelectric multiferroics possess both the magnetic and ferroelectric orders in one phase[1]. Substantial ME effect can be derived through fabricating composites of a ferroelectric (FE) and a ferromagnetic (FM) material in the form composites [2]. We have used homogenization theory for the analysis of the external field (electrical or magnetic) applied on a magnetoelectric composite and the resultant polarization and magnetization responses which are vital in its use as new devices. When the period of the structure is very small, a direct numerical approximation of the solution to magnetoelectric problem may be prohibitive, or even impossible. Here homogenization provides an alternative scheme of approximating such solutions by means of a function which solves the problem corresponding to a "homogenized" material. Homogenization method deals with the asymptotic analysis of partial differential equations in heterogeneous materials with a periodic structure, when the characteristic length  $\epsilon$  of the period tends to zero.

## II. THEORY

### A. Asymptotic homogenization

A two-scale asymptotic homogenization analysis combined with a variational formulation is developed for determination of the equivalent material properties of a periodic multiferroic magnetoelectric composite. Local and average (global) electrical, magnetic, and mechanical constitutive behaviour are computed. For a linear magneto-electro-elastic solid, constitutive equations are governed by the electrical,

mechanical and magnetic fields. The model quantifies the local electrical and magnetic potential, displacements, electrical and magnetic fields, stress and strain fields, magnetization (through magnetic flux density) and polarization (through electric displacement) and von-Mises stress, besides the effective magneto-electro-mechanical properties. The mathematical theory of homogenization accommodates the phase interaction in characterising both the macro and micro-mechanical behaviours of the composite material. i.e., the method permits the introduction of different field equations in a microscopic scale to each constituent of a composite while following the representative volume element (RVE) notion. Let  $\Omega$  be a fixed domain in  $\mathbf{x}$ -space. We consider an auxiliary  $\mathbf{y}$ -space divided into parallelepiped periods  $\mathbf{Y}$ . The linear constitutive relations for small deformations for multiferroics in the absence of heat flux are given by

$$\sigma_{ij} = C_{ijkl}^{EH} \epsilon_{kl} - e_{kij} E_k - e_{kij}^M H_k \quad (S1)$$

$$D_i = e_{ijk} \epsilon_{jk} + \kappa_{ij}^{EH} E_j + \alpha_{ij} H_j \quad (S2)$$

$$B_i = e_{ijk}^M \epsilon_{jk} + \alpha_{ji} E_j + \mu_{ij}^{EH} H_j \quad (S3)$$

Here  $\sigma$ ,  $\epsilon$ ,  $\mathbf{D}$ ,  $\mathbf{B}$  are stress, strain, displacement, body force, mass density, electric displacement vector, and magnetic flux density respectively.  $\mathbf{C}^{EH}$ ,  $\mathbf{e}$ ,  $\mathbf{e}^M$ ,  $\kappa^{EH}$  and  $\mu^{EH}$  are stiffness, strain to (electric, magnetic) field coupling constants (or piezo-electric and -magnetic coefficients), permittivity (dielectric) and (magnetic) permeability respectively. Considering the standard homogenization procedure, the material functions  $\mathbf{C}^{EH}$ ,  $\mathbf{e}$ ,  $\mathbf{e}^M$ ,  $\kappa^{EH}$  and  $\mu^{EH}$ , are considered to be  $\mathbf{Y}$ -periodic functions in the unit cell domain defined as  $\mathbf{Y} = [0, Y_1] \times [0, Y_2] \times [0, Y_3]$  [3]. The functions involved in this expansion are assumed to be dependent on these two variables, where one (i.e.,  $\mathbf{x}$ ) describing the "global" or average response of the structure and the other (i.e.,  $\mathbf{y}$ ) describing the "local" or microstructural behaviour [4]. Here the two sets of variables  $\mathbf{x}$  and  $\mathbf{x}/\epsilon$  take into account the two scales of the homogenization; the  $\mathbf{x}$  variable is the macroscopic variable, whereas

---

\* kpjayachandran@gmail.com

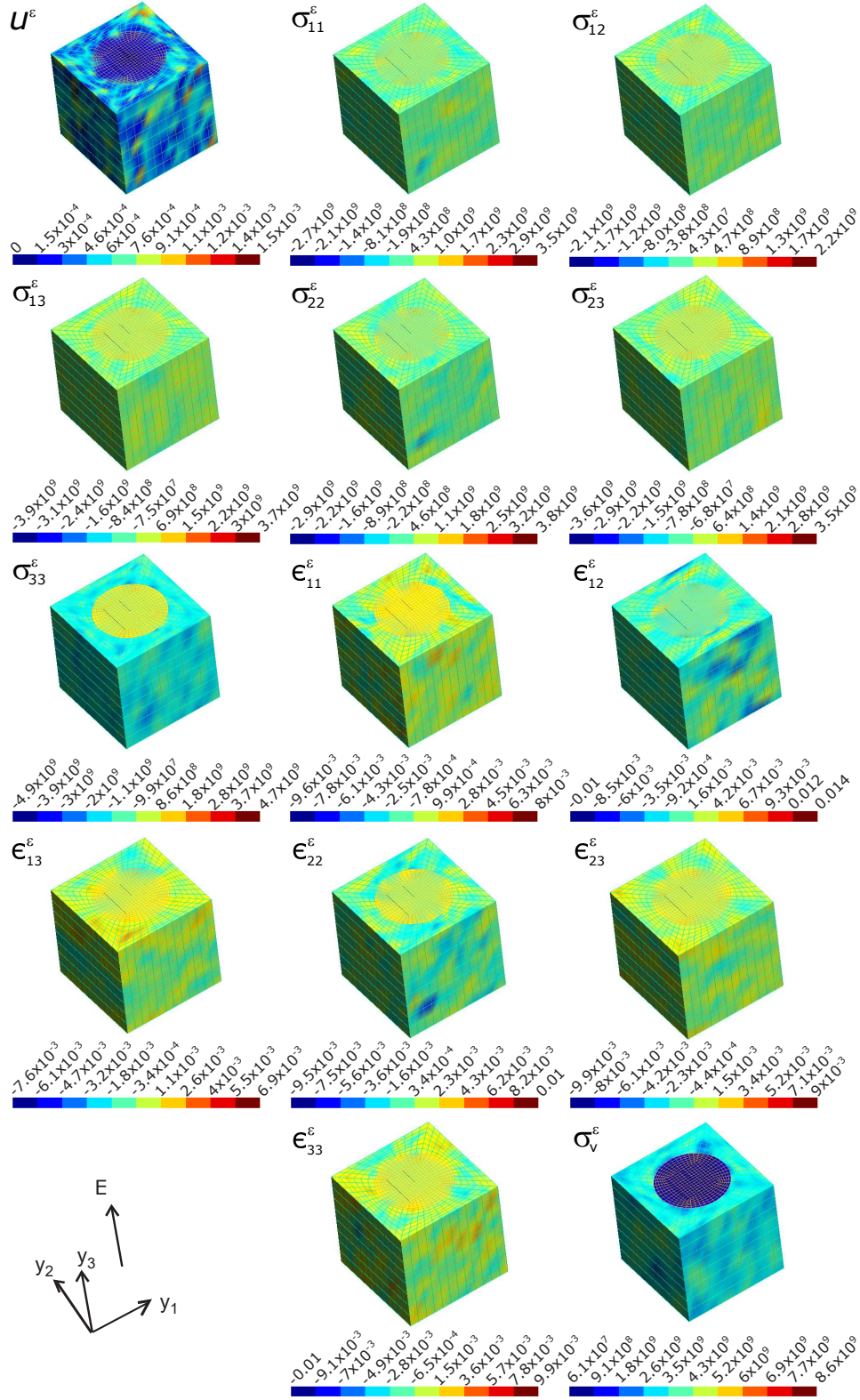


Figure S1. Map of local fields (computed at the nodal points of the FEM) of magnetoelectric composite BaTiO<sub>3</sub>–CoFe<sub>2</sub>O<sub>4</sub>, *viz.*, the stress  $\sigma_{ij}^E$  ( $N/m^2$ ), strain  $\epsilon_{ij}^E$ , the equivalent von Mises stress  $\sigma_v^E$  ( $N/m^2$ ), and displacement  $u^E$  ( $m$ ) upon applying a global electric field  $\mathbb{E}$  of  $10^8 V/m$  on the unit cell. Here the magnetic CoFe<sub>2</sub>O<sub>4</sub> cylindrical pillars are surrounded by ferroelectric BaTiO<sub>3</sub> matrix and both are aligned towards the  $y_3$  axis of the local coordinate system.

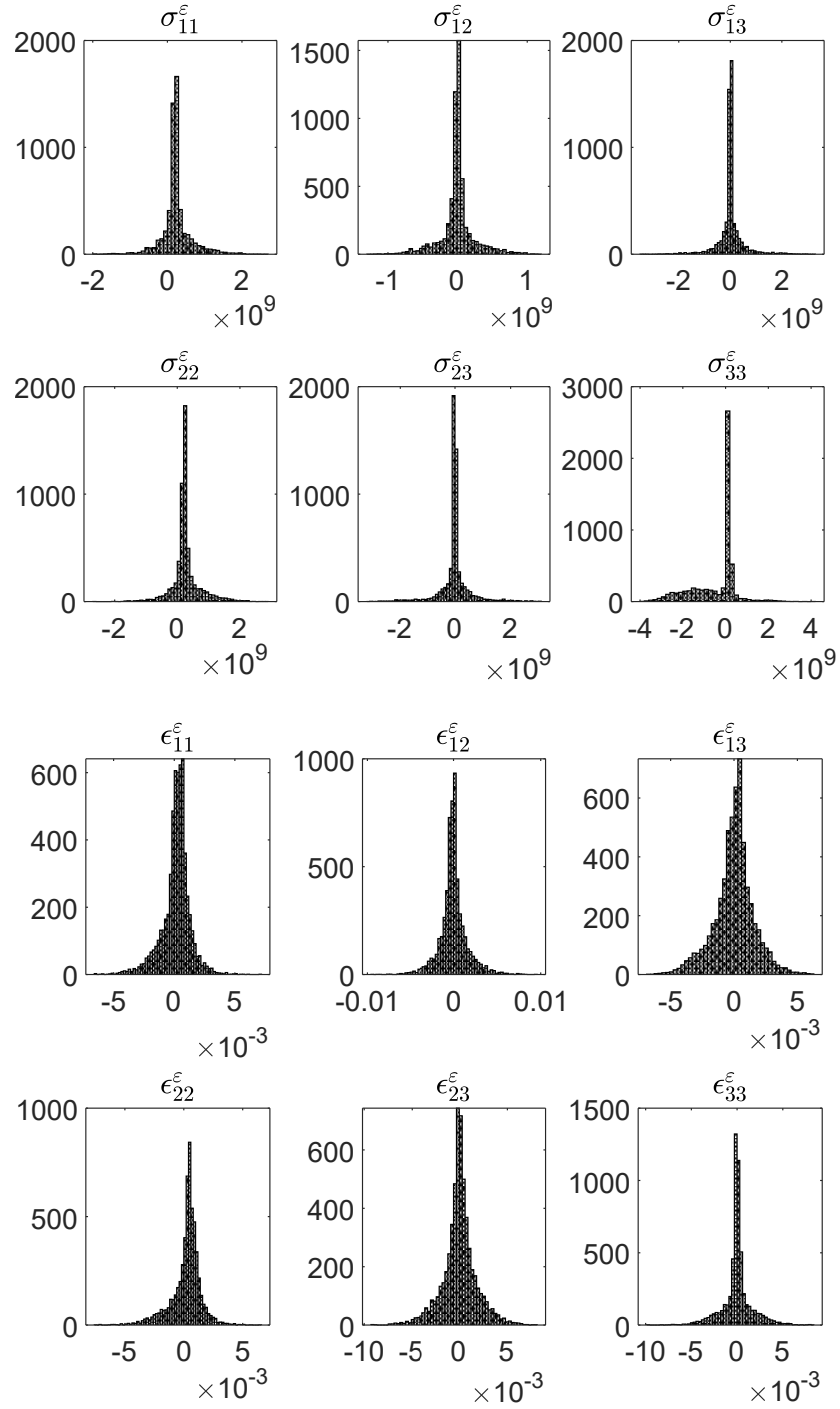


Figure S2. Histogram of the local stress ( $\sigma_{ij}^\epsilon$ ) and strain ( $\epsilon_{ij}^\epsilon$ ) values consequent to the application of external electric field (averaged over finite elements).

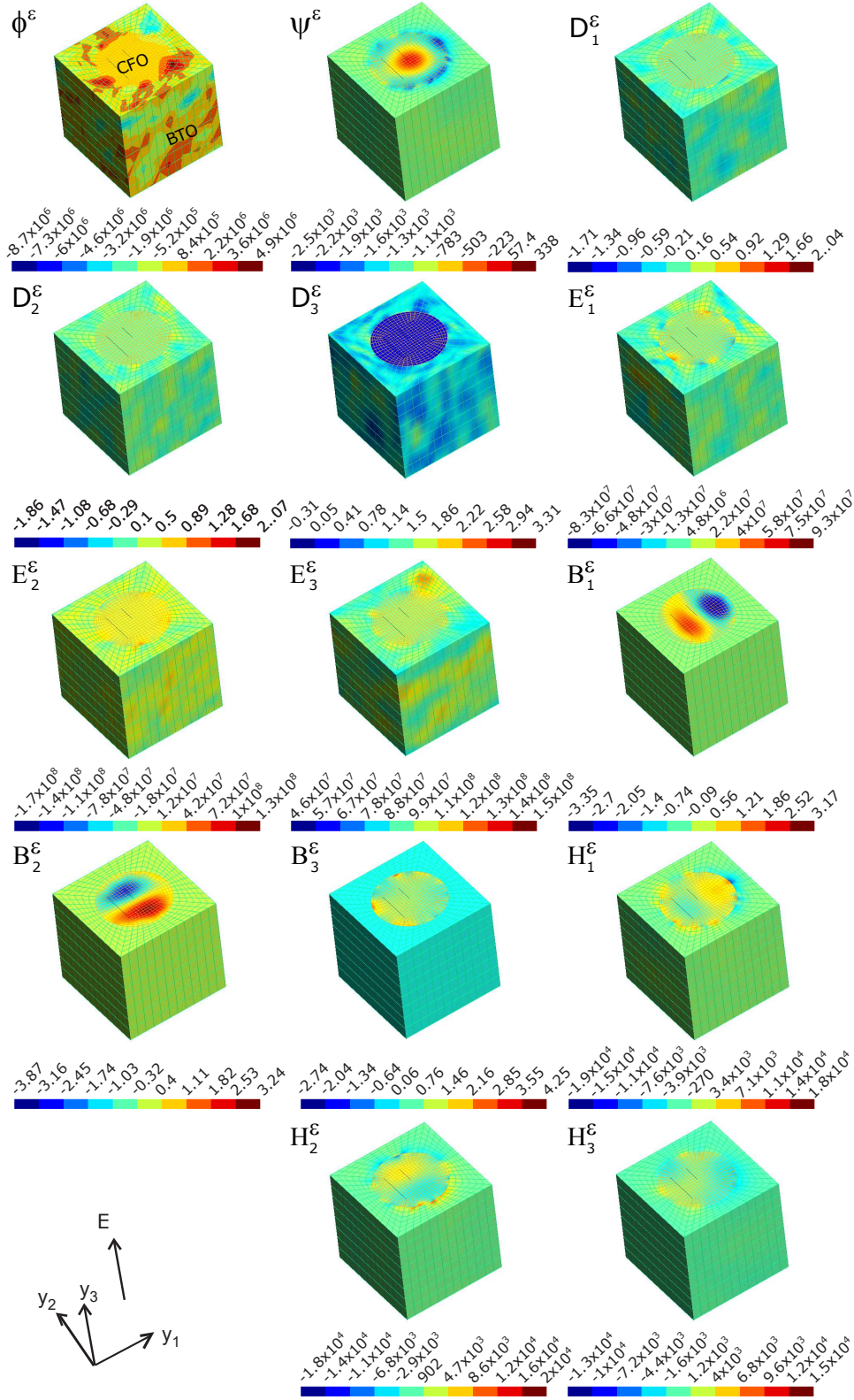


Figure S3. Map of local magnetic scalar potential  $\psi^\epsilon$  (A), electric potential  $\phi^\epsilon$  (V), electric field  $E_j^\epsilon$  (V/m), magnetic field  $H_j^\epsilon$  (A/m), electric displacement  $D_3^\epsilon$  (C/m<sup>2</sup>), and magnetic flux  $B_3^\epsilon$  (Wb/m<sup>2</sup>) computed at the nodal points of the FEM, upon applying a global electric field  $E$  of  $10^8$  V/m on a magnetoelectric composite of BaTiO<sub>3</sub>-CoFe<sub>2</sub>O<sub>4</sub>.

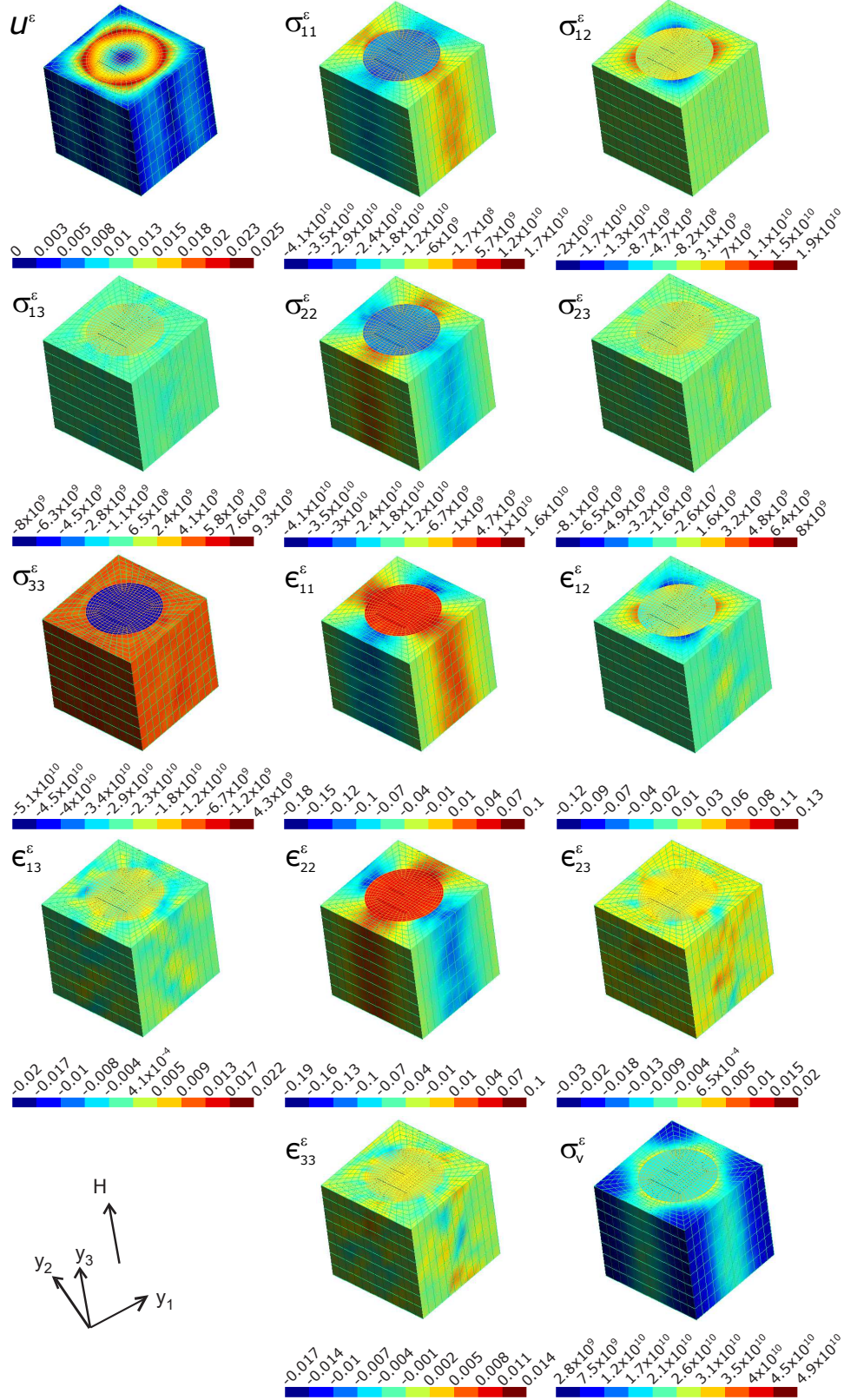


Figure S4. Map of local fields (computed at the nodal points of the FEM) of magnetolectric composite BaTiO<sub>3</sub>–CoFe<sub>2</sub>O<sub>4</sub>, *viz.*, the stress  $\sigma_{ij}^e$  ( $N/m^2$ ), strain  $\epsilon_{ij}^e$ , the equivalent von Mises stress  $\sigma_v^e$  ( $N/m^2$ ), and displacement  $u^e$  ( $m$ ) upon applying a biasing magnetic field  $H$  of  $10^8 A/m$  on the unit cell. Here the magnetic CoFe<sub>2</sub>O<sub>4</sub> cylindrical pillars are surrounded by ferroelectric BaTiO<sub>3</sub> matrix and both are aligned towards the  $y_3$  axis of the local coordinate system.

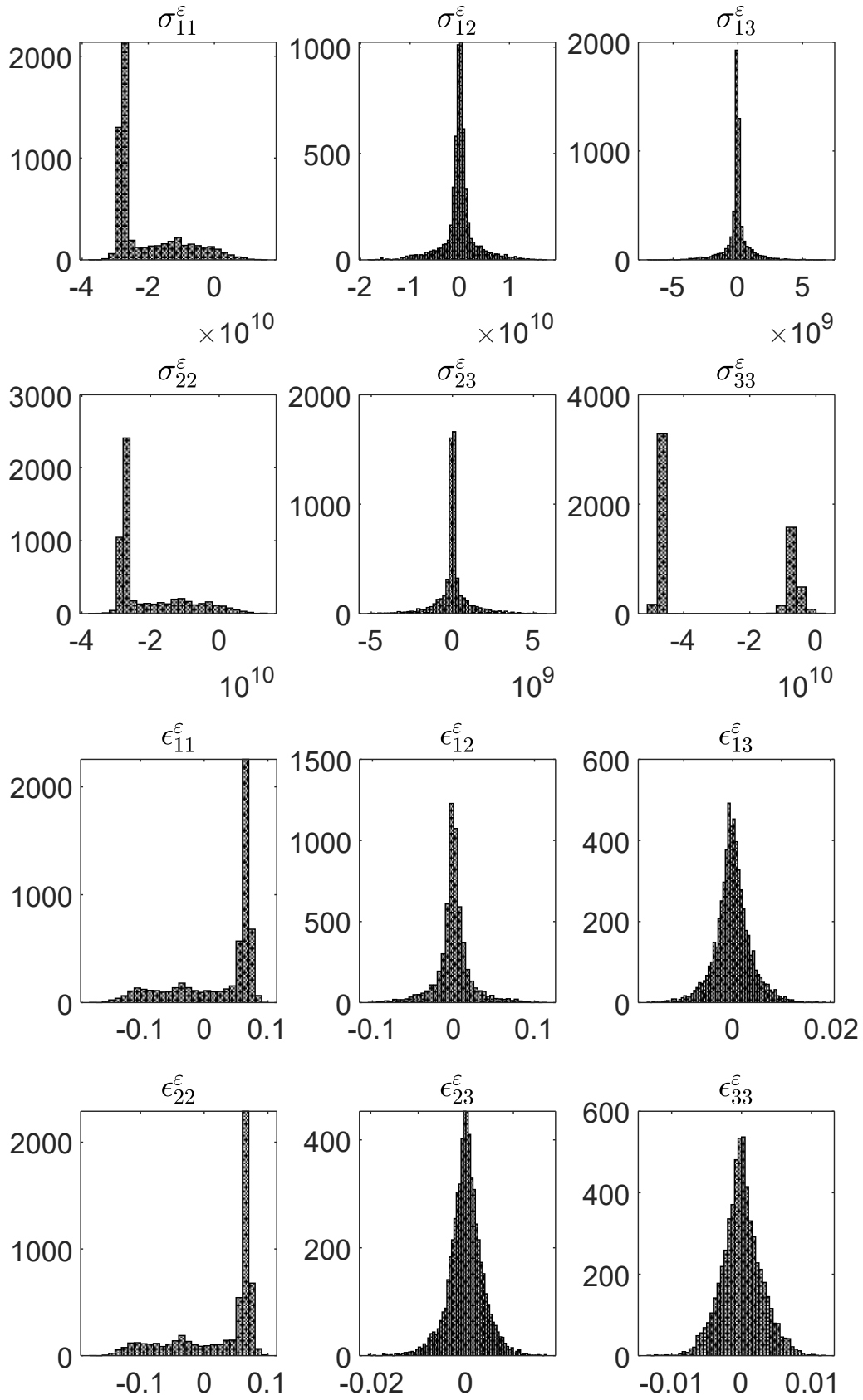


Figure S5. Histogram of the local stress ( $\sigma_{ij}^\varepsilon$ ) and strain ( $\epsilon_{ij}^\varepsilon$ ) values consequent to the application of external magnetic field (averaged over finite elements).

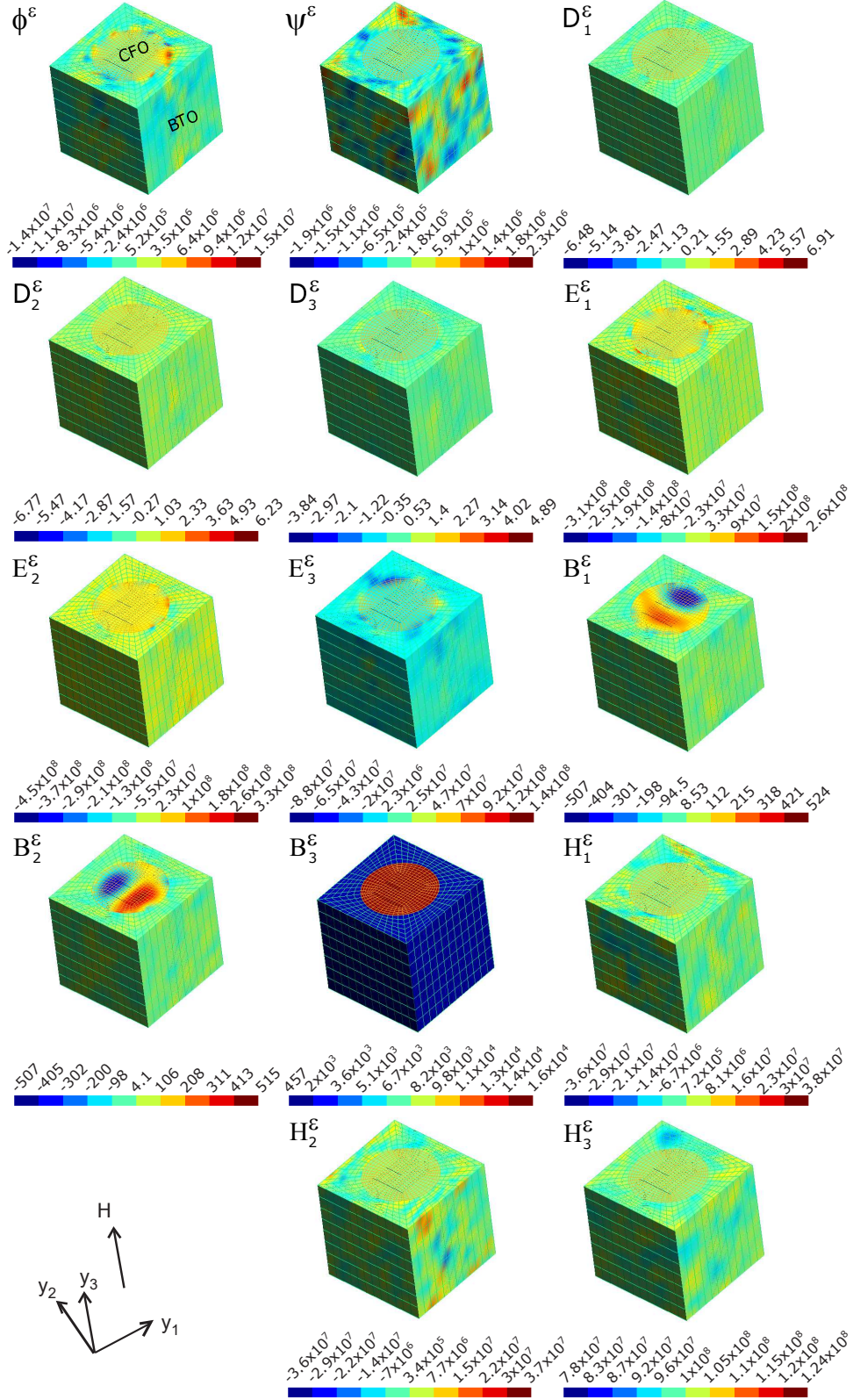


Figure S6. Map of local electric potential  $\phi^\epsilon$  (V), magnetic scalar potential  $\psi^\epsilon$  (A), electric field  $E_j^\epsilon$  (V/m), magnetic field  $H_j^\epsilon$  (A/m), electric displacement  $D_3^\epsilon$  (C/m<sup>2</sup>), and magnetic flux  $B_3^\epsilon$  (Wb/m<sup>2</sup>) computed at the nodal points of the FEM, upon applying a biasing magnetic field  $H$  of  $10^8$  A/m on a magnetoelectric composite of BaTiO<sub>3</sub>-CoFe<sub>2</sub>O<sub>4</sub>.

the  $\mathbf{x}/\varepsilon$  variable takes into account the *microscopic* geometry.

The detailed theoretical analysis is given elsewhere in a previous publication [3]. The local strain  $\epsilon_{ij}^\varepsilon(\mathbf{x})$ , electric field  $E_j^\varepsilon(\mathbf{x})$  and the magnetic field  $H_j^\varepsilon(\mathbf{x})$  too can be obtained once the homogenized macroscopic problem is solved.

$$\begin{aligned} \epsilon_{ij}^\varepsilon(\mathbf{x}) &= \epsilon_{ij}^0(\mathbf{x}) + \frac{\partial \eta^{mn}(\mathbf{x}, \mathbf{y})}{\partial y_j} \\ &\times \epsilon_{mn}(u^0(\mathbf{x})) + \frac{\partial R^m(\mathbf{x}, \mathbf{y})}{\partial y_j} \frac{\partial \varphi^0(\mathbf{x})}{\partial x_m} \\ &+ \frac{\partial \Psi^m(\mathbf{x}, \mathbf{y})}{\partial y_j} \frac{\partial \psi^0(\mathbf{x})}{\partial x_m} \end{aligned} \quad (\text{S4})$$

$$\begin{aligned} E_j^\varepsilon(\mathbf{x}) &= - \left[ \frac{\partial \varphi^0(\mathbf{x})}{\partial x_j} + \frac{\partial \eta^{mn}(\mathbf{x}, \mathbf{y})}{\partial y_j} \right. \\ &\times \epsilon_{mn}(u^0(\mathbf{x})) + \frac{\partial R^m(\mathbf{x}, \mathbf{y})}{\partial y_j} \frac{\partial \varphi^0(\mathbf{x})}{\partial x_m} \\ &\left. + \frac{\partial \Psi^m(\mathbf{x}, \mathbf{y})}{\partial y_j} \frac{\partial \psi^0(\mathbf{x})}{\partial x_m} \right] \end{aligned} \quad (\text{S5})$$

$$\begin{aligned} H_j^\varepsilon(\mathbf{x}) &= - \left[ \frac{\partial \psi^0(\mathbf{x})}{\partial x_j} + \frac{\partial \lambda^{mn}(\mathbf{x}, \mathbf{y})}{\partial y_j} \right. \\ &\times \epsilon_{mn}(u^0(\mathbf{x})) + \frac{\partial \Theta^m(\mathbf{x}, \mathbf{y})}{\partial y_j} \frac{\partial \varphi^0(\mathbf{x})}{\partial x_m} \\ &\left. + \frac{\partial Q^m(\mathbf{x}, \mathbf{y})}{\partial y_j} \frac{\partial \psi^0(\mathbf{x})}{\partial x_m} \right] \end{aligned} \quad (\text{S6})$$

The microscopic stress  $\sigma_{ij}^\varepsilon(\mathbf{x})$ , electrical displacement  $D_i^\varepsilon(\mathbf{x})$  and magnetic flux densities  $B_i^\varepsilon(\mathbf{x})$  at each point of the domain can be computed using the constitutive equations (S1)–(S3), and the field equations as

$$\begin{aligned} \sigma_{ij}^\varepsilon(\mathbf{x}) &= C_{ijkl}^\varepsilon(\mathbf{x}) \left( \frac{\partial u_k^0(\mathbf{x})}{\partial x_l} + \frac{\partial u_k^1(\mathbf{x}, \mathbf{y})}{\partial y_l} \right) \\ &- e_{kij}^\varepsilon(\mathbf{x}) \left( - \frac{\partial \varphi^0(\mathbf{x})}{\partial x_k} - \frac{\partial \varphi^1(\mathbf{x}, \mathbf{y})}{\partial y_k} \right) \\ &- e_{kij}^{M\varepsilon}(\mathbf{x}) \left( - \frac{\partial \psi^0(\mathbf{x})}{\partial x_k} \right. \\ &\left. - \frac{\partial \psi^1(\mathbf{x}, \mathbf{y})}{\partial y_k} \right) \end{aligned} \quad (\text{S7})$$

$$\begin{aligned} D_i^\varepsilon(\mathbf{x}) &= e_{ijk}^\varepsilon(\mathbf{x}) \left( \frac{\partial u_j^0(\mathbf{x})}{\partial x_k} + \frac{\partial u_j^1(\mathbf{x}, \mathbf{y})}{\partial y_k} \right) \\ &+ \kappa_{ij}^{\varepsilon H}(\mathbf{x}) \left( - \frac{\partial \varphi^0(\mathbf{x})}{\partial x_j} - \frac{\partial \varphi^1(\mathbf{x}, \mathbf{y})}{\partial y_j} \right) \\ &+ \alpha_{ij}^{\varepsilon E}(\mathbf{x}) \left( - \frac{\partial \psi^0(\mathbf{x})}{\partial x_j} - \frac{\partial \psi^1(\mathbf{x}, \mathbf{y})}{\partial y_j} \right) \end{aligned} \quad (\text{S8})$$

$$\begin{aligned} B_i^\varepsilon(\mathbf{x}) &= e_{ijk}^{M\varepsilon}(\mathbf{x}) \left( \frac{\partial u_j^0(\mathbf{x})}{\partial x_k} + \frac{\partial u_j^1(\mathbf{x}, \mathbf{y})}{\partial y_k} \right) \\ &+ \alpha_{ji}^{\varepsilon E}(\mathbf{x}) \left( - \frac{\partial \varphi^0(\mathbf{x})}{\partial x_j} - \frac{\partial \varphi^1(\mathbf{x}, \mathbf{y})}{\partial y_j} \right) \\ &+ \mu_{ij}^{\varepsilon E}(\mathbf{x}) \left( - \frac{\partial \psi^0(\mathbf{x})}{\partial x_j} \right. \\ &\left. - \frac{\partial \psi^1(\mathbf{x}, \mathbf{y})}{\partial y_j} \right) \end{aligned} \quad (\text{S9})$$

The average fields are computed to be

$$\begin{aligned} \langle \sigma_{ij} \rangle &= \tilde{C}_{ijkl}^{EH} \left( \frac{\partial u_k^0(\mathbf{x})}{\partial x_l} \right) + \tilde{e}_{kij} \left( \frac{\partial \varphi^0(\mathbf{x})}{\partial x_k} \right) \\ &+ \tilde{e}_{kij}^M \left( \frac{\partial \psi^0(\mathbf{x})}{\partial x_k} \right) \end{aligned} \quad (\text{S10})$$

$$\begin{aligned} \langle D_i \rangle &= \tilde{e}_{ijk} \left( \frac{\partial u_j^0(\mathbf{x})}{\partial x_k} \right) - \tilde{\kappa}_{ij}^{\varepsilon H} \left( \frac{\partial \varphi^0(\mathbf{x})}{\partial x_j} \right) \\ &- \tilde{\alpha}_{ij} \left( \frac{\partial \psi^0(\mathbf{x})}{\partial x_j} \right) \end{aligned} \quad (\text{S11})$$

$$\begin{aligned} \langle B_i \rangle &= \tilde{e}_{ijk}^M \left( \frac{\partial u_j^0(\mathbf{x})}{\partial x_k} \right) - \tilde{\alpha}_{ji} \left( \frac{\partial \varphi^0(\mathbf{x})}{\partial x_j} \right) \\ &- \tilde{\mu}_{ij}^{\varepsilon E} \left( \frac{\partial \psi^0(\mathbf{x})}{\partial x_j} \right) \end{aligned} \quad (\text{S12})$$

The above macroscopic equations (i.e. they do not contain  $\mathbf{y}$ ) can be computed once the homogenized solution for  $\mathbf{u}^0$ ,  $\varphi^0$  and  $\psi^0$  and that of the corresponding fields *viz.*,  $\frac{\partial u_j^0(\mathbf{x})}{\partial x_k}$ ,  $\frac{\partial \varphi^0(\mathbf{x})}{\partial x_j}$  and  $\frac{\partial \psi^0(\mathbf{x})}{\partial x_j}$  are prescribed.

### III. NUMERICAL IMPLEMENTATION

We have developed a programming platform called POSTMAT (*material postprocessing*) in this work for the solution of the microscopic system of equations resulting from homogenization and the details are given elsewhere [3, 5]. A three-dimensional (3D) multiferroic finite element is conceived with five degrees of freedom (DOF)-three DOFs for spatial displacements and one each for electric and magnetic potentials. Eight-noded isoparametric elements with  $2 \times 2 \times 2$  Gauss-point integration are used to obtain solutions. Altogether there were nine microscopic equations that should be solved for as much number of unknowns namely the characteristic functions  $\chi_i^{mn}$ ,  $\eta^{mn}$ ,  $\lambda^{mn}$ ,  $R^m$ ,  $\Phi_i^m$ ,  $\Theta^m$ ,  $Q^m$ ,  $\Psi^m$  and  $\Gamma_k^m$ , where the indices  $m, n = 1, 2, 3$  [3]. The problem is reduced to standard variational FEM, after the usual approximations of finite element formulation

and can be expressed concisely as  $\mathbf{K}\mathbf{u} = \mathbf{f}$  where  $\mathbf{K}$  is the global stiffness matrix,  $\mathbf{u}$  is the vector of unknown functions and  $\mathbf{f}$  is the load vector. Magneto-electric multiferroic material, in general, can be considered as an aggregate of single crystalline crystallites/grains and hence the system altogether would be polycrystalline nature. The unit cell or the representative volume element (RVE) conceived in this work is a volume containing a sufficiently large number of crystallites or grains that its properties can be considered as equivalent to that of the macroscopic sample. The electric polarization  $\mathbf{P}$  as well as the magnetization  $\mathbf{M}$  interspersed inside the crystallites could be mapped using using some coordinate system. In a sense the underlying crystal orientation can encompass the orientations of  $\mathbf{P}$  or  $\mathbf{M}$ . Thus we introduce the Euler angles  $(\varphi, \theta, \psi)$  to quantify the crystal orientations of a multiferroic polycrystal (Fig. S1), as the crystallites in an as-grown sample are randomly oriented in the lattice space and hence require three angles to describe its orientation with reference to a fixed coordinate system. Here we use the so called *x-convention*, where the first and third rotation is through the  $y$ -axis (here it is  $y_2$ -axis) and the second rotation is through the intermediate  $x$ -axis (here it is  $y_1$ -axis). Thus all the physical quantities  $\gamma'_{ijklmn\dots}(\mathbf{y}')$  expressed in a crystallographic coordinate system  $\mathbf{y}'$  would be coordinate-transformed to the local coordinate system  $\mathbf{y}$  according to the following scheme

$$\gamma_{ijkl\dots}(\mathbf{y}) = e_{im}e_{jn}e_{kp}e_{lq}\dots\tilde{\gamma}'_{mnpq\dots}(\mathbf{y}') \quad (\text{S13})$$

before it is introduced for homogenization. (i.e., the FE and FM materials' electromechanical property data entered into the homogenization program are obtained with respect to the crystallographic coordinates.) Here  $e_{\mu\nu}$  are the Euler transformation matrices [6].

For FEM simulation of the homogenization, a multiferroic crystallite is represented by a finite element in the microstructure. Thus we have a polycrystalline unite cell having as much number of crys-

tallites as the number of finite elements by which it is discretized. As-grown FE (or for that matter FM) polycrystal, often ends up in a near complete compensation of polarization (or magnetization) and the material consequently exhibit very small, if any, electric (or magnetic) effect until they are poled by the application of an electric (magnetic) field. The orientation distribution of the crystallites (grains) in such a polycrystalline material would be uniform with a standard deviation  $\sigma \rightarrow \infty$  before poling (application of electric/magnetic field) and that after poling would best be represented by a distribution function with  $\sigma \rightarrow 0$ . Thus, any pragmatic configuration of orientation distribution of grains in multiferroic material would fit in a Gaussian distribution defined by the probability distribution function The convergence of magnetoelectric properties with unit cell size allows us to determine the simulation-space independent, equivalent magnetoelectric properties of the composite. Convergence analyses, on magnetoelectric composites reveal that accuracy one derives from discretizing the unit cell (in other words sampling of the unit cells with more number of grains or less number) is minimal above 1000 elements (grains) [7]. Consequently, we kept unit cells' sizes above 1000 finite elements in this study.

#### IV. RESULTS

Piezomagnetism drives materials to acquire magnetization upon application of mechanical stress. Since in BaTiO<sub>3</sub>-CoFe<sub>2</sub>O<sub>4</sub> composite system this phenomenon plays a crucial role in the overall magnetization that it acquires consequent to the electrical loading. The distribution of local (*microscopic*) fields *viz.*, the stress  $\sigma^\varepsilon$ , von Mises stress  $\sigma_v^\varepsilon$  and strain  $\epsilon^\varepsilon$  consequent to the application of an external electric field along the  $y_3$ -axis of the composite microstructure is displayed in Fig. S1. The histograms in Fig. S2 show the frequency of stress and strains that spread across the microstructure.

---

[1] H. Schmid, *Ferroelectrics* **162**, 317 (1994).  
[2] M. Avellaneda and G. Harshe, *J. Intell. Mater. Syst. Struct.* **5**, 501 (1994).  
[3] K. P. Jayachandran, J. M. Guedes, and H. C. Rodrigues, *J Intel Mat Syst Str* **25**, 1243 (2014).  
[4] E. Sanchez-Palencia, *Non-homogeneous media and vibration theory, Lecture notes in physics 127* (Springer-Verlag, Berlin, 1980).

[5] K. P. Jayachandran, J. M. Guedes, and H. C. Rodrigues, *Sci Rep* **10**, 1276 (2020).  
[6] H. Goldstein, *Classical Mechanics* (Addison-Wesley, Reading, MA, 1978).  
[7] K. P. Jayachandran, J. F. A. Madeira, J. M. Guedes, and H. C. Rodrigues, *Comp Mater Sci* **148**, 190 (2018), ISSN 0927-0256.